International Journal of Applied Chemistry.
ISSN 0973-1792 Volume 16, Number 1 (2020) pp. 35-51

https://dx.doi.org/10.37622/IJAC/16.1.2020.35-51

Study of the Factors Affecting the Heterogeneous Kinetics of Amorphous Ni Nanoparticles using the Simulation Method

Tuan Tran-Quoc [1], Dung Nguyen-Trong [2,*]

[1] *Faculty of Basic Science, University of Transport Technology, 54 Trieu Khuc, Thanh Xuan, Ha Noi, Viet Nam*

[2] *Faculty of Physics, Hanoi National University of Education, 136 Xuan Thuy, Cau giay, Ha Noi, Viet Nam.*

Abstract

The content of the article studies heterogeneous kinetics of amorphous Ni nanoparticles with atomic number (N), N = 2048 atoms (Ni_{2048}), 2916 atoms (Ni_{2916}), 4000 atoms (Ni_{4000}), 5324 atoms (Ni_{5324}), 6912 atoms (Ni_{6912}), 8788 atoms (Ni_{8788}) at temperature (T), T = 300 K with heating rate 10^6 K/s; Ni_{5324} at T = 300 K with heating rate: $5x10^5$ K/s to 10^6 K/s, $5x10^6$ K/s, 10^7 K/s, $5x10^7$ K/s, 10^8 K/s; Ni_{5324} at T = 300 K, 400 K, 500 K, 600 K, 700 K, 900 K, 1100 K, 1300 K with heating rate 10^6 K/s by Molecular dynamics (MD) simulation method with Sutton-Chen (SC) embedded interaction potential and free boundary conditions. The result of heterogeneous kinetics determined through the radial distribution function (RDF), coordinate number (CN), energy (E) size (D), and glass transition temperature (T_g) through the relationship between E and T. The result shows that the first peak position (r) of RDF which has value change is r = 2.55 Å, CN = 13, T_g = 630 K, D is always proportional (~) with $N^{-1/3}$, E ~ N^{-1}. It shows that T_g of amorphous Nanomaterials is smaller than T_g of crystalline Nanomaterials; T_g of crystalline Nanomaterials is smaller than T_g of bulk materials; and confirms that the great influence of factors on the inhomogeneous dynamics of amorphous Ni nanoparticles.

Keywords: Atomic number, heating rate, temperature, amorphous Ni nanoparticles, heterogeneous kinetics, molecular dynamics.

1. INTRODUCTION

Today, Nanomaterials have been widely applied in the fields of chemistry, physics, materials, pharmaceuticals, and agriculture [1-4]. Nickel (Ni) is one of the most preeminent materials among Nanomaterials. Ni is a silvery-white metal, hard, malleable and metal in the ferromagnetic group. At normal conditions, Ni is stable in the air, formed two states crystalline & amorphous, and inert with oxygen. In recent years, the amorphous Ni Nano-materials have been used in many fields of science and technology such as applying as a coating material in biomedical, electronic, mechanical, optical [5], photocatalytic [6], solar battery [7, 8], electrical, optical, biochemical and biomedical [9, 10]. To study and make amorphous Ni Nanomaterials, researchers used many methods such as theoretical method, experimental method, and simulated method [11]. For the theoretical method, using the Mean-Field Theory (MFT) [12], the Effective Field Theory (EFT) [13], the Green Function Theory (GFT) [14, 15], the Monte Carlo (MC) Method [16], the Contingent Valuation Method (CVM) [17] and Bethe model [18]. With experimental method using by chemical control reduction [19], hydrothermal [20], Ethanol-Water System (EWS) [21], electrochemical [22], Sol-gel [23], Polyol [24], Atomic Force Microscope (AFM) analysis [25], AFM data [26]. With simulated method using by Molecular Dynamics (MD) method [27-29] in these cluster Ni metal [30-38]. The result shows that the size (D) of amorphous Ni Nano-materials is smaller than $D < 30$ nm [39] then amorphous Ni Nanomaterials have many new properties compared to Ni bulk materials such as coercive (λ) reduction. Amorphous Ni Nano-materials will be having the transition from ferromagnetic state to Atomically Precise Manufacturing (APM). X. He, et al shows the Curie phase transition temperature (T_c) of amorphous Ni Nano-materials increases from $T_c = 593$ K to $T_c = 612$ K, 622 K, 626 K, 627 K while the size (D) increases from D = 24 nm to D = 50 nm, 96 nm, 165 nm, 200 nm [40], T_c is always lower than $T_c = 631$ K of Ni bulk material [41], and there is abnormal in absorption spectra, photocatalyst of metal and nonmetal [42]. When the density of Ni atoms increases which leads to a transition from a metallic state to a nonmetal state [43], a bandgap of amorphous Ni nanoparticles explodes compared to crystalline materials [44]. In the deformation process, the stress of the amorphous surface layer will be reduced resulting in the crystallization's delay process compared to the bulk material [45]. Recently, Amodeo and J. Amodeo, et al have given that, with the Molecular Dynamics (MD) method, most studies have shown the influence of size and shape on the crystallization of Ni nanoparticles [46]. Gerberich, et al. have used Scanning Electron Microscope (SEM) and MD method to study the effect of the oxide layer surface on the mechanical properties in a material [47]. Han, et al. [48] with the Transmission Electron Microscope (TEM) method show the influence of the surface on the experimental measurement results. With the surface layer of nanoparticles is an amorphous material that has a great influence on the deformation and shape of nanoparticles [49] with a new understanding of the refractive index, the dielectric constant of a material is a very important basis for studying new materials [50]. Recently, there have been many studies on amorphous Ni nanoparticles structure [51] and Al [52], and conditions of metal transition [53]. In particular, Ni nanoparticles have the greatest crystalline capacity due to its high melting point, so Ni nanoparticles

are used as electrodes to detect glucose [54]. To control the size and shape of nanoparticles, researchers used heterogeneous catalysts [55-58]. With Li et al., particles are smaller than 3 nm obtained by the increasing temperature (T) from T = 363 K to T = 453 K [59], and La prune, et al. [60] obtained particles which is smaller than 2 nm and Goodarzi, et al. [61] Besides, Wen, et al. that glass transition temperature (T_g) of the nanowires is always proportional (~) to the D^{-1} [62]; When atoms number (N) increases then phase transition temperature (T_m) increases [63], $D \sim N^{-1/3}$ results match with the simulation results of Fe bulk [64], crystallize Ni nanoparticles [65]. In this, $T_m \sim N^{-1/3}$, $T_m \sim D^{-1}$ [66- 71], and other results with $D \sim N^{-1/3}$ [37, 38, 62, 67- 71]. When N increases from N = 336 atoms to N = 8007 atoms, then T_m increases from T_m=980 K to T_m=1380 K [63], T_g = 800 K with N = 4000 atoms [72] the result is completely consistent with experimental research results of amorphous Ni Nanomaterials in the range from T_g = 403 K to T_g = 523 K [73], easy to crystallize, increase in size at T = 493 K, stable at T = 523 K [74]. Besides, with the result of heterogeneous kinetics of amorphous Ni Nano-materials which studied a bit such as the experimental method T. Ichikawa has determined that the closest interconnection distance of Ni bulk is r = 2.43 Å [75], simulation method Dung. N.T, et al., with crystallized Ni nanoparticles is r = 2.45 Å [65] and P.H. Kien with amorphous Ni nanoparticles is r = 2.52 Å [76]. This means that the glass transition temperature of amorphous Ni not only depends on the cluster size but also other related factors such as shape and dimension [36]. Basing on the given result of the structural characteristics and the glass transition temperature of Ni Nanomaterials, combined with our recent studies on the structure of Nanomaterials such as Fe, Ni [64, 65, 77], Al [78], we continue studying the affection of factors on the heterogeneous kinetics of amorphous Ni nanoparticles by the molecular dynamics (MD) method [79]. The newly obtained results are expected to be the orientation basis for future empirical studies.

2. CALCULATION OF METHODS

Randomly sow the atoms of amorphous Ni nanoparticles into spherical blocks with size (D), $\rho=\frac{N}{V} \rightarrow D=2\left(\frac{3N}{4\pi\rho}\right)^{\frac{1}{3}}$ (1) with density (ρ), ρ = 7.81 g.cm^{-3}, atoms numbers (N) by Molecular dynamics (MD) simulation method of interaction potential Pak-Doyama (PD) (1) and free boundary condition [27-29], $\varphi(r) = a(r+b)^4 + c(r+d)^2 + e$ (1)

In which r_{ij} is the linking distance between atoms; φ(r) is the interaction potential; a, b, c, d, e are constants there and r_c is cut radius. For the parameters with values shown in Table 1.

Table 1: Parameters of amorphous Ni nanoparticles

Parameters	a	b	c	d	e	r_c(Å)
Ni	-0.12929	-1.82709	1.16473	-2.50849	-0.135705	3.6

Initially create amorphous Ni nanoparticles with atomic number (N), N = 2048 atoms

(Ni_{2048}), 2916 atoms (Ni_{2916}), 4000 atoms (Ni_{4000}), 5324 atoms (Ni_{5324}), 6912 atoms (Ni_{6912}), 8788 atoms (Ni_{8788}) at the temperature (T), T = 300 K with a heating rate of 10^6 K/s, the time for each step of MD simulation is 0.46 fs. Then, increase heating speed from $5x10^5$ K/s to 10^6 K/s, $5x10^6$ K/s, 10^7 K/s, $5x10^7$ K/s, 10^8 K/s with Ni_{5324} at T = 300 K; temperature increase from T = 300 K to T = 500 K, 600 K, 700 K, 900 K, 1100 K with Ni_{5324} and a heating rate of 10^6 K/s. To study heterogeneous kinetics of amorphous Ni nanoparticles, using Molecular dynamics (MD) simulation method, Verlet algorithm, the average coordination number (CN), $CN=4\pi\rho\int_0^{r_1} g(r)r^2dr$, the heating process by the laws of Nos´e [80], Hoover [81], the defined radial distribution function (RDF) of the amorphous Ni nanoparticles [82-86]. The radial distribution function (RDF), $g(r)=\frac{n(r)}{4\pi r^2 dr\rho_0}$ r_1 is the first position of RDF and E is energy, n is the atomic number, ρ is atomic density [87, 88], and crystallization temperature (T_g) through the relationship between E and T. To check the accuracy of results, it is necessary to do this through tools as a centrosymmetric parameter [70, 89], bond angle analysis [90], bond order analysis [91], AFM analysis method which used to determine the morphology of the surface [25], fractal and multi-fractal geometric structures, determined directly from the database [26].

3. RESULTS AND DISCUSSIONS.

3.1 Effect of heating rate.

To study the effect of heating rate, selected Ni_{5324} and identified structural features with different heating rates shown in Figure 1, Table 2.

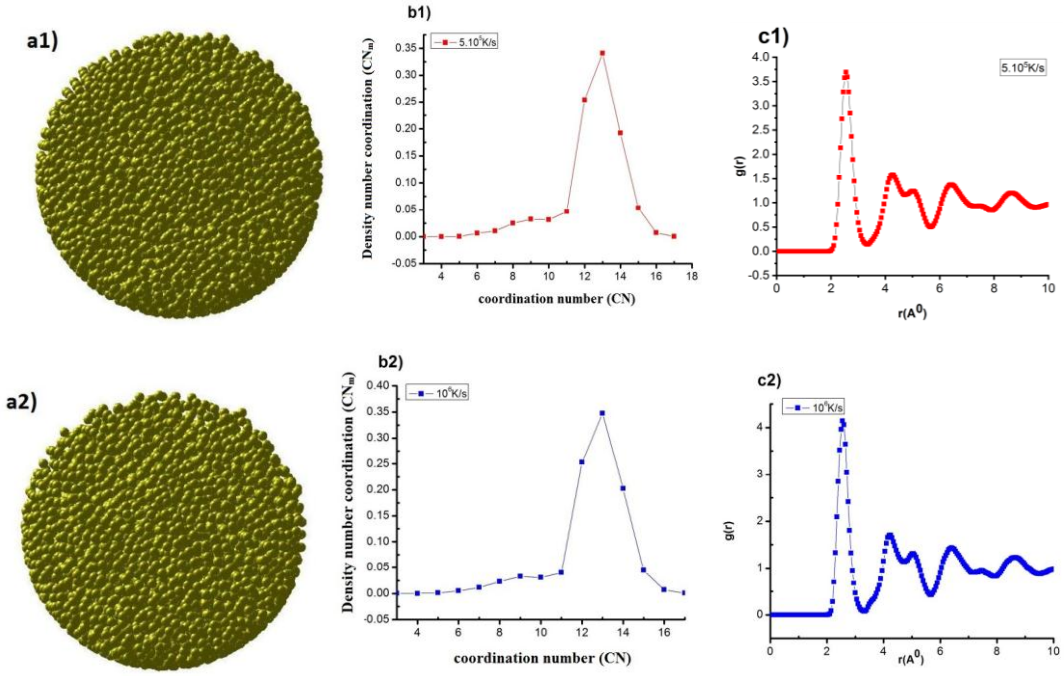

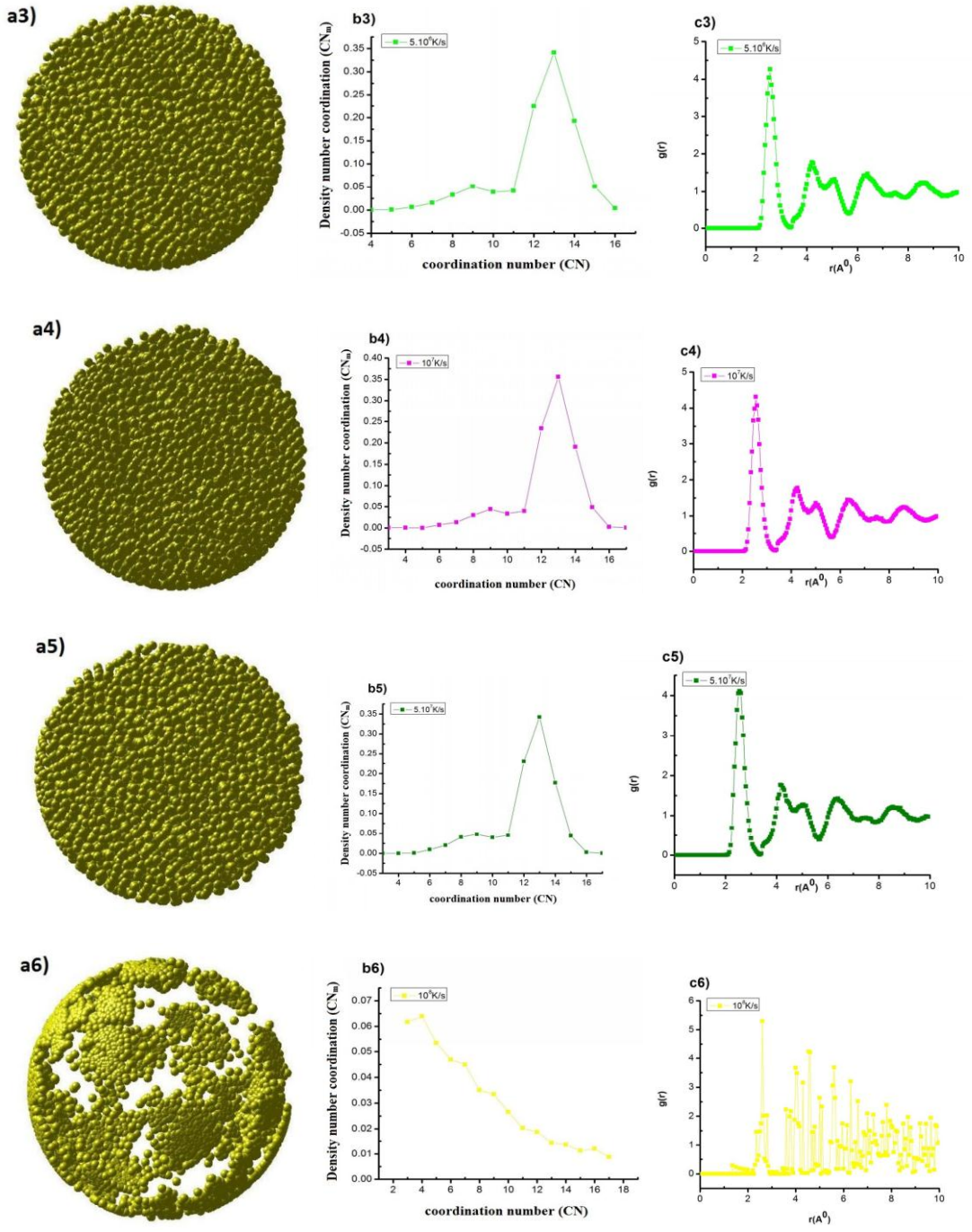

Figure 1: The structural characteristics of amorphous Ni_{5324} nanoparticles as shape (a1, a2,., a6), coordination numbers (b1, b2, .., b6), radial distribution function (c1, c2, .., c6) with different heating rates.

Table 2: Size and energy of amorphous Ni_{5324} nanoparticles with different heating rates.

heating speed (K/s)	5.10^5	10^6	5.10^6	10^7	5.10^7	10^8
D (nm)	2.6	2.6	2.6	2.6	2.61	16.04
E(eV)	-0.725	-0.731	-0.811	-0.779	-0.865	169.119

The results show amorphous Ni_{5324} nanoparticles with a heating rate of $5x10^5$ K/s are spherical shaped, shown by yellow (Figure 1a1) with size (D), D = 2.6 nm, energy (E), E = -0.725 eV (Table 2); coordinate numbers (CN), CN = 13, the density coordination number (CN_m), CN_m = 33.82% (Figure 1b1). The first position (r) of the radial distribution function (RDF) has value r = 2.55 Å, the first peak height of RDF g(r), g(r) = 3.69 (Figure 1c1). When increasing heating rate $5x10^5$ K/s to 10^6 K/s, $5x10^6$ K/s, 10^7 K/s, $5x10^7$ K/s, 10^8 K/s leads to the shape of amorphous Ni_{5324} nanoparticles change (Figures 1a1, 1a2, ..1a6); Coordinate number CN is the constant, CN = 13 and the density coordination number has varied change from CN_m = 33.82% to CN_m = 35.6% (Figure 1b1, Figure 1b2, .., Figure 1b6); The first peak position has to value a constant with r = 2.55Å and the height of the radial distribution function varied change from g(r) = 3.69 to g(r) = 5.20 (Figure 1c1, Figure 1c2, .., Figure 1c6); D increased from D = 2.6nm to D = 16.04nm, broken structure shape at heating rate 10^8 K/s, E decreased from E = -0.725 eV to E = -0.889 eV and then increased from E = -0.889 eV to E = 169.119 eV (Table 2) shows that when increasing heating rate leads to D increase, the density of atoms decreases and the result is very useful for experimental research results in the future.

3.2 Effect of atomic number.

Next, studying the effect of the atomic number on heterogeneous kinetics of amorphous Ni nanoparticle shown in Figure 2.

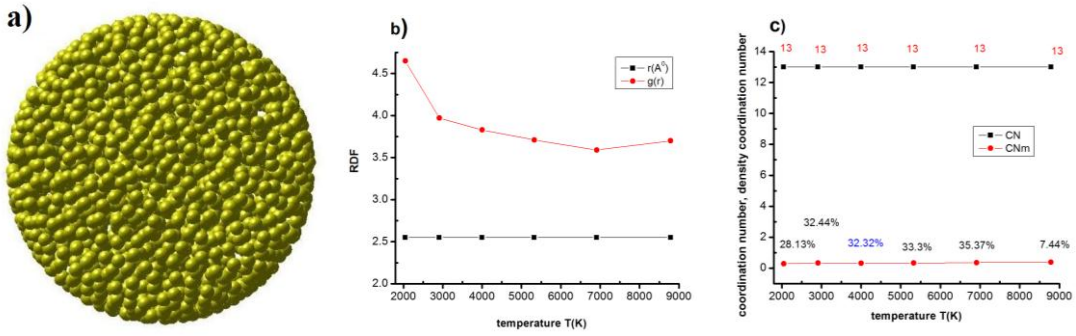

Figure 2: The structural characteristics of amorphous Amorphous Ni nanoparticles such as Ni_{2048} nanoparticle shape (a), radial distribution function (b), coordination number (c) with different atomic numbers.

The results show the spherical form of amorphous Ni_{2048} nanoparticles has a spherical shape, the atoms uniformly distributed, shown by the yellow color (Figure 2a); r = 2.55 Å and the first peak height RDF has a value of g(r) = 4.65; coordination number (CN), CN = 13 and density coordination number (CN_m), CN_m = 28.13%. When increasing atoms number (N) from Ni_{2048} to Ni_{2912}, Ni_{4000}, Ni_{5324}, Ni_{6912}, Ni_{8788}, then the shape of amorphous Ni nanoparticles changes, the size (D) increases from D = 3.74 nm to D = 4.20 nm, 4.51 nm, 5.03 nm, 5.42 nm, 5.91 nm, energy (E) decreases from E = -0.657 eV to E = -0.664 eV, -0.675 eV, -0.674 eV, -0.684 eV, -0.679 eV, -0.710 eV; The first peak position of RDF has the constant value r = 2.55 Å, the given results are entirely consistent with simulation results with amorphous Ni Nanomaterials is r = 2.52 Å [76], this shows that the bonding length between Ni-Ni of amorphous material is always greater than the linking length of bulk material with r = 2.43 Å [75] of Ni bulk by the experimental method, r = 2.45 Å [65] of crystallize Ni by simulation method and has value twice the covalent radius is 1.21 Å [47], the reason is that in the crystalline state or bulk material, the energy of the system decreases leading to the reduction in the bonding length, so the bonding length is always smaller than the bonding length of amorphous Ni. Besides, g(r) decreases from g(r) = 4.65 to g(r) = 3.97, 3.83, 3.71, 3.59, 3.70 (Figure 2b); the number of the coordinate number has a constant value is CN = 13, the density coordinate number CN_m decreases from CN_m = 28.13% to CN_m = 27.79% (Figure 2c) which proves that when increasing atoms number leads to the density of atoms increases and that confirms a huge influence of size D on the structure of amorphous Ni nanoparticles. Also, the change in the height value of the first vertex RDF change of the first peak value of g(r) with D. The value of g(r) reaches the maximum value is g(r) = 4.65 when size D = 3.74 nm and the smallest value g(r) = 3.59 when size D = 5.42 nm caused by the structural heterogeneity in amorphous Ni nanoparticles. Besides, there is a relationship between size (D) and energy (E) with atomic number (N) of amorphous Ni nanoparticles, the relationship between quantities D with N and E with N, the result shown in Figure 3.

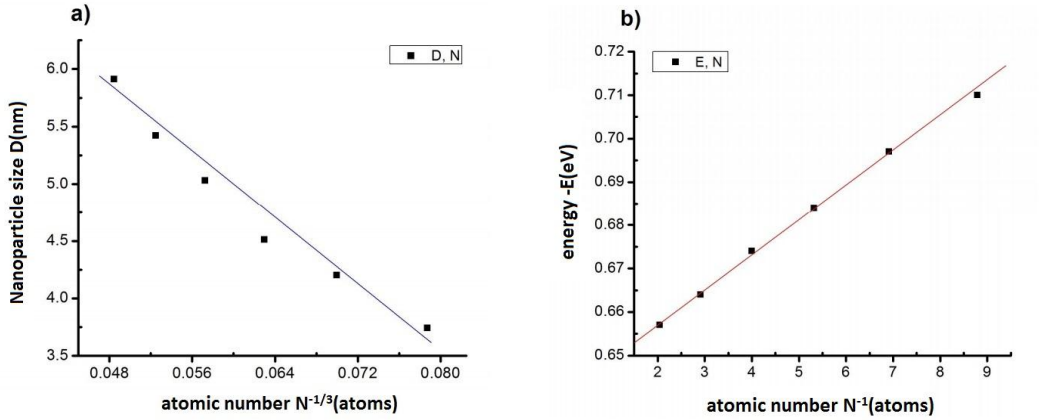

Figure 3: The relationship between nanoparticles size D, atoms number N (a), energy E, and atoms number N (b) of amorphous Ni nanoparticles.

The given results show that when increasing atoms number (N), the size (D) of amorphous Ni nanoparticles increases linearly and shown by the blue line (Figure 3a); energy (E) decreases linearly and shown by the red line (Figure 3b). The relationship between D with N and E with N determined by the formula $D = 9.117 - 69.993N^{-1/3}$, $E = 0.748 + 240N^{-}$ which shows that D is always proportional (~) to $N^{-1/3}$, $E \sim N^{-1}$, the results are consistent with the previous results $D \sim N^{-1/3}$ [37, 38, 62, 67- 71] as simulation results of Fe bulk and Fe nanoparticles [64], crystallize Ni nanoparticles [65], the results got are the basis for future empirical studies.

3.3 Influence of temperature.

Next, studying the effect of temperature on heterogeneous kinetics of amorphous Ni nanoparticle shown in Figure 4.

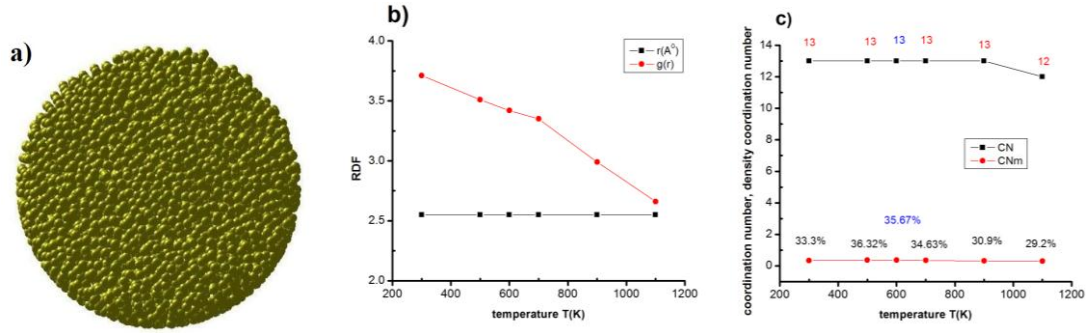

Figure 4: The structural characteristics of amorphous Ni nanoparticles such as amorphous Ni_{5324} nanoparticle shape (a), radial distribution function (b), coordination number (c) with different temperatures.

The results show that the amorphous Ni_{5324} nanoparticles at (T), T = 300 K has the spherical shape, size D = 2.6 nm, E = -0.679 eV, the atoms uniformly distributed, shown in yellow (Figure 4a); the r position of RDF is r = 2.55 Å and g(r) = 3.71; coordination number (CN), CN = 13 and density coordination number (CN_m), CN_m = 33.3%. When increasing the temperature (T) from T = 300 K to T = 500 K, 600 K, 700 K, 900 K, 1100 K, the shape of amorphous Ni nanoparticles changes, D has a constant value with D = 2.6nm, E increases from E = -0.679eV to E = -0.655eV, -0.622eV, -0.578eV, -0.478eV, -0.361eV; r has a constant value with r = 2.55 Å, g(r) decreases from g(r) = 3.71 to g (r) = 3.51, 3.42, 3.35, 2.99, 2.66 (Figure 4b); the coordination number decreases from CN = 13 to CN = 12, with CN = 12 at T = 1100 K, the density coordination number CN_m decreases from CN_m = 33.3% to CN_m = 29.2% (Figure 4c) that proves when increasing temperature leads to a decrease in the density of atoms. To confirm that, study the glass transition temperature of amorphous Ni_{5324} nanoparticles in Figure 5.

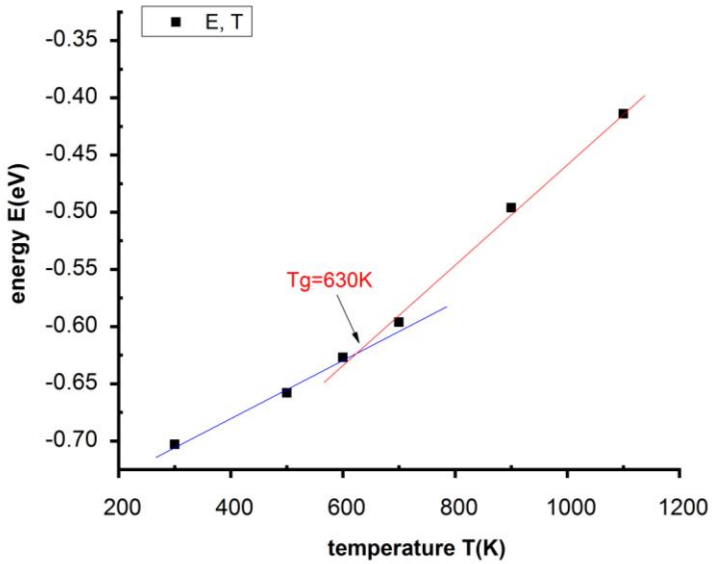

Figure 5: The glass transition temperature of amorphous Ni_{5324} nanoparticles.

The results show that when T increases leading to E increases, in the range from T = 300 K to T = 600 K, E increases slightly, shown by the blue line. With T > 700 K, then E increases linearly, shown by the red line, the intersection at the point T = 630 K proves that this point is the crystallization point and called the glass transition temperature (T_g), T_g = 630 K (Figure 5), the result accordance with the results previously published T_g = 631K [40, 41], the results were consistent with experimental research results of amorphous Ni Nanomaterials in the range from T_g = 403 K to T_g = 523 K [73], easy to crystallize, increase in size at T = 493 K, stable at T = 523 K [74]. Besides, this result is also consistent with $T_g \sim N^{-1/3}$, and when N increases, the phase transition temperature (T_m) increases, [63, 72], $T_m \sim D^{-1}$ [66- 71], this shows that the T_g of amorphous Ni depends not only on the D but also on other related factors such as shape, structural state [36]. It shows that T_g = 630 K of amorphous Ni nanoparticles always smaller T_g = 800 K of Ni nanoparticles in the crystalline state [65] and Ni bulk, and has a very large effect of temperature on the structure, the phase transition of amorphous Ni nanoparticle and the cause is because of the side effects and surface effects cause. When increases T, then E_{tot} increases, leading to an atomic density decrease. Now, to explain that T_g of amorphous Nanomaterials are smaller than T_g of crystalline Nanomaterials, and T_g of crystalline Nanomaterials are smaller than T_g of bulk materials [65] need to do with in-depth research tools such as centrosymmetric parameter [70, 89], to solve this conundrum. To confirm the accuracy of the results, it is necessary to deploy them on specialized tools: Centrosymmetric parameter [70, 89], bond angle analysis [90], bond order analysis [91], AFM analysis method used to determine the morphology of the surface [25], fractal and multi-fractal geometric structures, determined directly from the database [26] and with the current results considered a very useful basis for future empirical research results.

4. CONCLUSION

Results of the study the effect of heating rate, the number of atoms, temperature on heterogeneous kinetics of amorphous Ni nanoparticle shows that The amorphous Ni nanoparticles got spherical shaped, size nanoscale, expressed in yellow color. When increasing the heating rate from $5x10^5$ K/s to $1x10^8$ K/s, nanoparticle size increases, energy decreases and dramatically decreases, at 10^8 K/s heating speed leading to broken amorphous Ni nanoparticles. When increasing the number of atoms leads to a size D increase in proportional to $N^{-1/3}$ and E energy decreases proportional to N^{-1}, these results are consistent with the published results [37, 38, 62, 67-71] and results simulation results of Fe bulk and Fe nanoparticles [64], crystallize Ni nanoparticles [65]. The values of the radial distribution function (RDF) has a constant value of r = 2.55 Å, the first peak height of RDF g(r) has an increasing value when increasing atomic number (N); coordinates number (CN) has CN constant value is CN=13, density coordinates number (CNm) has value change is negligible, the given results are entirely consistent with simulation results with amorphous Ni Nano materials is r = 2.52 Å [76], while with bulk material r = 2.43 Å [75], crystallize material r = 2.45 Å [65] and covalent radius (r) is r = 1.21 Å [47] this shows that the bonding length between Ni-Ni of amorphous material is always greater than the linking length of Ni bulked and confirmed Ni nanoparticles at temperature (T), T = 300, 500, 700, 900, 1100 K always have an amorphous structure, CN always has a constant value, CN = 13, has a glass transition temperature (T_g), T_g = 630 K, the result accordance with the results previously published T_g = 631 K [40, 41], experimental research results of amorphous Ni nanoparticles at T_g = 403 K to T_g = 523 K [73], easy to crystallize, increase in size at T=493 K, stable at T = 523 K [74]. Besides, this result is also consistent with $T_g \sim N^{-1/3}$, and when N increases then phase transition temperature (T_m) increases [63, 72], $T_m \sim D^{-1}$ [66-71], this shows that the Tg of amorphous Ni depends not only on the D but also on other related factors such as shape, structural state [36]. The results show that T_g = 630 K of amorphous Ni nanoparticles always smaller T_g = 800 K of Ni nanoparticles in the crystalline state [65] and has a very large effect of temperature on the structure, the phase transition of amorphous Ni nanoparticle, the cause is because of the side effects and surface effects cause, with this research result, it is to consolidate the future experimental results.

ACKNOWLEDGMENT

I thank computer room, faculty of physics of Hanoi National University of Education, Viet Nam has created all favorable conditions, help me throughout the process of calculating, simulating and finishing the content of the article.

REFERENCES

[1] Țălu, Ș., Bramowicz, M., Kulesza, S., Ghaderi, A., Dalouji, V., Solaymani, S., Fathikenari, M., Ghoran-neviss, M., Fractal features and surface micromorphology of diamond nanocrystals, J. Microsc, 2016b, 264, 143–152.

[2] Majidi, S., Achour, A., Rai, D.P., Nayebi, P., Solaymani, S., Nezafat, N.B., Elahi, S.M., Efect of point defects on the electronic density states of SnC nanosheets: frst-principles calculations, Results Phys, 2017, 7, 3209–3215.

[3] Mahdavi, S., Nano-TiO2 modifed with natural and chemical compounds as efcient adsorbents for the removal of Cd+2, Cu+2, and Ni+2 from water, Clean Technol. Environ. Policy, 2016, 18, 81–94.

[4] Solaymani, S., Ghoranneviss, M., Elahi, S.M., et al., The relation between structural, rugometric and fractal characteristics of hard dental tissues at micro and nano levels, Microsc. Res. Tech, 2019, 82, 421–428.

[5] Dalouji, V., Solaymani, S., Rezaee, S., Mehrparvar, D.: Nonmetal-metal transition in carbon films embed-ded by Ni nanoparticles: the temperature coefcient of resistivity (TCR), Raman spectra and surface morphology, Optik, 2018b, 156, 338–345.

[6] Taiga Yu rino,Yohei Ueda, Yo shiki Shimizu, Shinji Tanaka, Haruka Nishiyama, Hayato Tsurugi, Kazuhiko Sato, and Kazushi Mashima, Salt-Free Reduction of Nonprecious Transition - Metal Compounds: Generation of Amorphous Ni Nanoparticles for Catalytic C–C Bond, Formation, Angew. Chem. Int .Ed, 2015, 54 ,1 4437–14441

[7] Y. Ruan, C. Wang and J. Jiang, Nanostructured Ni compounds as electrode materials towards high-performance electrochemical capacitors, J. Mater. Chem. A, 2016, 4, 14509-14538.

[8] L.Gaouyat, Z.He, J.-F.Colomer, D.Schryvers, F.Mirabella and O. Deparis, In Linking Optical Properties and Nanostructure of NiCrOx Cermet Nanocomposite for Solar Thermal Application, ed. B. Di Bartolo, J.Collins and L.Silvestri, Springer Netherlands, Dordrecht, 2015, 497-497

[9] Xu, R., Xie, T., Zhao, Y. and Li, Y., Quasi-homogeneous catalytic hydrogenation over monodisperse nickel and cobalt nanoparticles, Nanotechnology, 2007, 18, 055602.

[10] Wang, D.P., Sun, D.B., Yu, H.Y., Qiu, Z.G., and Meng, H.M., Preparation of one-dimensional nickel nanowires by self-assembly process, Materials Chemistry and Physics, 2009, 113, 227-232.

[11] H. Kachkachi, Effects of spin non-collinearities in magnetic nanoparticles, Journal of Magnetism and Magnetic Materials, 2007, 316 (2), 248–254.

[12] F. Michael, C. Gonzalez, V. Mujica, M. Marquez, M. A. Ratner, Size dependence of ferromagnetism in gold nanoparticles: Mean field results, Physical Review B, 2007, 76 (22), 224409.

[13] W. Jiang, H. yu Guan, Z. Wang, A. bang Guo, Nanoparticle with a ferrimagnetic interlayer coupling in the presence of single ion anisotropis, Phys. B: Condens. Matter, 2012, 407 (3), 378–383.

[14] A. Zaim, M. Kerouad, Monte carlo simulation of the compensation and critical

behaviors of a ferrimagnetic core/shell nanoparticle ising model, Physica A: Statistical Mechanics and its Applications, 2010, 389(17), 3435-3442.

[15] Y. Y¨uksel, E. Aydıner, H. Polat, Thermal and magnetic properties of a ferrimagnetic nanoparticle with spin-3/2 core and spin-1 shell structure, Journal of Magnetism and Magnetic Materials, 2011, 323 (23), 3168–3175.

[16] L. Jiang, J. Zhang, Z. Chen, Q. Feng, Z. Huang, Monte carlo study of magnetic properties for the mixed spin-3/2 and spin-1 ferrimagnetic nanoparticles, Physica B: Condensed Matter, 2010, 405 (1), 420–424.

[17] H. Wang, Y. Zhou, D. Lin, C. Wang, Phase diagram of ising nano particles with cubic structures, Phys. Status Solidi (b), 2002, 232 (2), 254–263

[18] B. Deviren, M. Keskin, Y. Aydin, Compensation temperatures, magnetic susceptibilities and phase diagrams of a mixed ferrimagnetic ternary system on the 101 bethe lattice, JETP Letters, 2010, 92 (4), 214–222.

[19] Li, Y.D., Li, C.W., Wang, H.R., Li, L.Q. and Qian, Y.T, Preparation of nickel ultrafine powder and crystalline film by chemical control reduction, Materials Chemistry Physics, 1999, 59, 88-90.

[20] Li, Y.D., Li, L.Q., Liao, H.W. and Wang, H.R, Preparation of pure nickel, cobalt, nickel-cobalt and nickel-copper alloys by hydrothermal reduction, Journal of Materials Chemistry, 1999, 9, 2675-2677.

[21] Zheng, H., Liang, J., Zeng, J. and Qian, Y., Preparation of nickel nanopowders in ethanol-water system (EWS), Materials Research Bulletin, 2001, 36, 947-952.

[22] Zach, M.P., and Penner, R.M., Nanocrystalline Nickel Nanoparticles, Advanced Materials, 2000, 12, 12

[23] S. Devarajan, P. Bera, S. Sampath, Bimetallic nanoparticles: a single step synthesis, stabilization, and characterization of Au–Ag, Au–Pd, and Au–Pt in sol–gel derived silicates, J. Colloid Interface Sci, 2005, 290, 117.

[24] Couto, G.G, Klein, J.J, Schreiner, W.H., Mosca, D.H., Oliveira and Zarbin., Ni nanoparticles obtained by a modified polyol process: Synthesis, characterization and magnetic properties, Journal of colloid and Interface science, 2007, 311, 461-468.

[25] Țălu, Ș., Bramowicz, M., Kulesza, S., Dalouji, V., Solaymani, S., Valedbagi, S., Fractal features of carbon–nickel composite thin flms, Microsc. Res. Tech, 2016a, 79, 1208–1213.

[26] Țălu, Ș., Bramowicz, M., Kulesza, S., Dalouji, V., Ilkhani, M., Ghaderi, A., Solaymani, S., Infuence of annealing process on surface micromorphology of carbon–nickel composite thin flms, Opt. Quantum Electron, 2017, 49, 204.

[27] B. T. H. L. Khanh, V. V. Hoang and H. Zung, Structural properties of amorphous Fe2O3 nanoparticles, Eur. Phys. J. D, 2008, 49, 325–332,

[28] H. M. Lu, W. T. Zheng, Q. Jiang, Saturation magnetization of ferromagnetic and ferrimagnetic [nanocrystals at room temperature, Journal of Physics D: Applied Physics, 2007, 40(2), 320–325.

[29] R.Yamamoto, T. Mihara, K. Taira, M. Doyama, Amorphous structures of iron obtained by quenching of the liquid state, Physics Letters A, 1979, 70, 1, 41–43.

[30] J. Lu and J. A. Szpunar, Applications of the embedded-atom method to glass formation and crystallization of liquid and glass transition-metal nickel, Philos. Mag. A, 1997, 75, 1057-1066.

[31] Y. Qi, T. Çağin, W. L. Johnson and W. A. Goddard III, Melting and crystallization in Ni nanoclusters: The mesoscale regime, J. Chem. Phys., 2001, 115, 385-394.

[32] Y.-H. Wen, Z.-Z. Zhu, R. Zhu and G.-F. Shao, Size effects on the melting of nickel nanowires: a molecular dynamics study, Phys. E, 2004, 25, 47-54.

[33] Y. Zhang, L. Wang and W. Wang, Thermodynamic, dynamic and structural relaxation in supercooled liquid and glassy Ni below the critical temperature, J. Phys.: Condens. Matter, 2007, 19, 196106.

[34] P. H. Kien, Molecular dynamics study of microscopic structures, phase transitions and dynamic crystallization in Ni nanoparticles, Mater. Sci., 2014, 2014, 253627.

[35] A. N. Andriotis, Z. G. Fthenakis and M. Menon, Correlated variation of melting and Curie temperatures of nickel clusters, Phys. Rev. B: Condens. Matter Mater. Phys., 2007, 75, 073413.

[36] H. M. Lu, P. Y. Li, Z. H. Cao and X. K. Meng, Size, shape, and dimensionality-dependent melting temperatures of nanocrystals, J. Phys. Chem. C, 2009, 113, 7598-7602

[37] Nguyen Trong Dung, Influence of impurity concentration, atomic number, temperature and tempering time on microstructure and phase transformation of Ni1-xFex (x = 0.1, 0.3, 0.5) nanoparticles, Modern Physics Letters B, 2018, 1850204 (14 pages).

[38] Tran Quoc Tuan, Nguyen Trong Dung, Effect of heating rate, impurity concentration of Cu, atomic number, temperatures, time annealing temperature on the structure, crystallization temperature and crystallization process of Ni1−x Cux bulk; x = 0.1, 0.3, 0.5, 0.7, International Journal of Modern Physics B, 2018, 32, 26, 1830009 (15 pages)

[39] Néel L., Théorie du trainage magnétique des ferromagnétiques en grains fins avec applications aux Terres Cuites, Annals of Geophysics, 1949, 5, 99 -136.

[40] X. He, H. Shi, Size and shape effects on magnetic properties of Amorphous Ni nanoparticles, Particuology, 2012, 10 (4), 497–502.

[41] C. Q. Sun, W. H. Zhong, S. Li, B. K. Tay, H. L. Bai, E. Y. Jiang, Coordination imperfection suppressed phase stability of ferromagnetic, ferroelectric, and superconductive nanosolids, The Journal of Physical Chemistry, 2004, 235B, 108 (3), 1080–1084.

[42] T. N. Rostovshchikova, M. I. Shilina, E. V. Golubina, E. S. Lokteva, I. N. Krotova, S. A. Nikolaev, K. I. Maslakov, D. A. Yavsin, Adsorption and oxidation of carbon monoxide on Au and Ni nanoparticles deposited on Al_2O_3 by laser electrodispersion, Russ. Chem. Bull., Int. Ed., 2015, 64, 812

[43] Nastaran Asareh, Vali Dalouji, Shahram Solaymani, Sahar Rezaee, Relation between carriers hopping rate and structural constants in amorphous carbon nickel flms with diferent nickel nanoparticles distributions, Optical and Quantum Electronics, 2019, 51:373, 1-11

[44] A. K. Gatin, M. V. Grishin, S. A. Gurevich, N. V. Dokhlikova, A. A. Kirsankin, V. M. Kozhevin, E. S. Lokteva, T. N. Rostovshchikova, S. Yu. Sarvadii, B. R. Shub and D. A. Yavsinc, Interaction of amorphous and crystalline nickel nanoparticles with hydrogen, Russian Chemical Bulletin, International Edition, 2015, 64, 10, 2337-2343.

[45] Alexandra M. Goryaeva, Claudio Fusco, Matthieu Bugnet, and Jonathan Amodeo, Influence of an amorphous surface layer on the mechanical properties of metallic nanoparticles under c ompression, Physical Review, 2019, 3, 033606.

[46] J. Amodeo and K. Lizoul, Mechanical properties and disloca-tion nucleation in nanocrystals with blunt edges, Mater. Des, 2017, 135, 223.

[47] Gerberich, E. B. Tadmor, J. Kysar, J. A. Zimmerman, A. M. Minor, I. Szlufarska, J. Amodeo, B. Devincre, E. Hintsala, and R. Ballarini, Review Article: Case studies in future trends of computational and experimental nanomechanics, J. Vac. Sci. Technol, 2017, A 35, 060801.

[48] W.-Z. Han, L. Huang, S. Ogata, H. Kimizuka, Z.-C. Yang, C. Weinberger, Q.-J. Li, B.-Y. Liu, X.-X. Zhang, J. Li, E. Ma, and Z.-W. Shan, From "smaller is stronger" to "size-independent strength plateau": Towards measuring the ideal strength of iron, Adv. Mater, 2015, 27, 3385.

[49] Alexandra M. Goryaeva, Claudio Fusco, Matthieu Bugnet, and Jonathan Amodeo, Influence of an amorphous surface layer on the m echanical properties of metallic nanoparticles under compression, Physical review materials, 2019, 3, 033606.

[50] Dalouji, V., Solaymani, S., Dejam, L., Elahi, S.M., Rezaee, S., Mehrparvar, D.: Gap states of ZnO thin flms by new methods: optical spectroscopy, optical conductivity and optical dispersion energy. Chin. Phys. Lett, 2018a), 35, 027701.

[51] S. Trady, M. Mazroui, A. Hasnaoui, and K. Saadouni, Molec-ular dynamics study of atomic-level structure in monatomic metallic glass, J. Non-Cryst.

Solids, 2016, 443, 136.

[52] S. Trady, A. Hasnaoui, M. Mazroui, and K. Saadouni, Lo-cal atomic structures of single-component metallic glasses, Eur.Phys.J.B, 2016, 89, 223.

[53] A. I. Fedorchenko, On the glass transition of the one-component metallic melts, J. Cryst. Growth, 2017, 475, 362.

[54] Yumei Peng, Qiong Chen, Jian Xie and Wei Lan, Communication-Facile Synthesis of Amorphous Nickel Boride Nanoparticles for Highly Sensitive Non-Enzyme Glucose Detection, Journal of the Electrochemical Society, 2019, 166, (6), B521-B523.

[55] M. Cargnello, Colloidal Nanocrystals as Building Blocks for Well-Defined Heterogeneous Catalysts, Chem. Mater., 2019, 31, 576–596.

[56] C. Vogt, E. Groeneveld, G. Kamsma, M. Nachtegaal, L. Lu, C. J. Kiely, P. H. Berben, F. Meirer and B. M. Weckhuysen, Unravelling structure sensitivity in CO_2 hydrogenation over nickel, Nat. Catal., 2018, 1, 127–134.

[57] J. Gao, Q. Liu, F. Gu, B. Liu, Z. Zhong and F. Su, RSC Adv., 2015, 5, 22759–22776.

[58] E. Zacharaki, P. Beato, R. R. Tiruvalam, K. J. Andersson, H. Fjellvåg and A. O. Sjåstad, From Colloidal Monodisperse Nickel Nanoparticles to Well-Defined Ni/Al_2O_3 Model Catalysts, Langmuir, 2017, 33, 9836–9843.

[59] Y. Li, J. Wen, A. M. Ali, M. Duan, W. Zhu, H. Zhang, C. Chen and Y. Li, Size structure–catalytic performance correlation of supported Ni/MCF-17 catalysts for CO_x-free hydrogen production, Chem. Commun., 2018, 54, 6364–6367.

[60] D. Laprune, A. Tuel, D. Farrusseng and F. C. Meunier, Highly Dispersed Nickel Particles Encapsulated in Multi - hollow Silicalite - 1 Single Crystal Nanoboxes: Effects of Siliceous Deposits and Phosphorous Species on the Catalytic Performances, ChemCatChem, 2017, 9, 2297–2307.

[61] F. Goodarzi, L. Kang, F. R. Wang, F. Joensen, S. Kegnaes and J. Mielby, Methanation of Carbon Dioxide over Zeolite - Encapsulated Nickel Nanoparticles, ChemCatChem, 2018, 10, 1566–1570.

[62] Y.-H. Wen, Z.-Z. Zhu, R. Zhu and G.-F. Shao, Size effects on the melting of nickel nanowires: a molecular dynamics study, Physica E: Low-dimensional Systems and Nanostructures, 2004, 25, 47 – 54.

[63] Y. Qi, T. Çağin, W. L. Johnson and W. A. Goddard III, Melting and crystallization in Ni nanoclusters: The mesoscale regime, J. Chem. Phys., 2001, 115, 385-394

[64] P.H. Kien, M.T. Lan, N.T. Dung, P.K. Hung, Anealing study of amorphous bulk and nanoparticle iron using molecular dynamics simulation, Int. J. Mod. Phys. B, 2014, 28 (23), 1450155.

[65] Trong Dung Nguyen, Chinh Cuong Nguyen and Vinh Hung Tran, Molecular dynamics study of microscopic structures, phase transitions and dynamic crystallization in Amorphous Ni nanoparticles, RSC Adv., 2017, 7, 25406–25413.

[66] Y.-H. Wen, Z.-Z. Zhu, R. Zhu and G.-F. Shao, Size effects on the melting of nickel nanowires: a molecular dynamics study, Phys. E, 2004, 25, 47-54

[67] Y. Qi, T. Çaˇgin, W. L. Johnson and W. A. Goddard III, Melting and crystallization in Ni nanoclusters: The mesoscale regime, The Journal of Chemical Physics, 2001, 115, 385-394;

[68] Y. Zhang, L. Wang and W. Wang, Thermodynamic, dynamic and structural relaxation in supercooled liquid and glassy Ni below the critical temperature, J. Phys.: Cond. Matt., 2007, 19, 196106.

[69] A. N. Andriotis, Z. G. Fthenakis and M. Menon, Correlated variation of melting and Curie temperatures of nickel clusters, Phys. Rev. B, 2007, 75, 073413.

[70] C. L. Kelchner, S. J. Plimpton and J. C. Hamilton, Dislocation nucleation and defect structure during surface indentation, Phys. Rev. B, 1998, 58, 11085–11088

[71] C. S. Tian, D. Qian, D. Wu, et. Body-Centered-Cubic Ni and Its Magnetic Properties, Phys. Rev. Lett., 2005, 94, 137210.

[72] Y. Zhang, L. Wang and W. Wang, Thermodynamic, dynamic and structural relaxation in supercooled liquid and glassy Ni below the critical temperature, J. Phys.: Condens. Matter, 2007, 19, 196106

[73] Sulekh Chandra, Avdhesh Kumar, Praveen Kumar Tomar Synthesis of Ni nanoparticles and their characterizations, Journal of Saudi Chemical Society, 2014, 18, 5, 437-442.

[74] Wilbert L. Vrijburg, Jolanda W.A. van Helden, Arno J.F. van Hoof, Heiner Friedrich, Esther Groeneveld, Evgeny A. Pidko, Emiel J.M. Hensen, Tunable colloidal Ni nanoparticles confined and redistributed in mesoporous silica for CO2 methanation, Catalysis Science & Technology, 2019, 175, 1-35.

[75] T. Ichikawa, Electron diffraction study of the local atomic arrangement in amorphous Iron and Nickel films, Physica Status Solidi (a), 1973, 19 (2), 707-716

[76] Pham Huu Kien, Study of structural transition of nickel metal under temperature, Phase Transitions, 2016, 90(7), 1-10.

[77] K. P. Huu, T. G. T. Thuy, H. P. Khac, The study of separation of crystal Fe and morphology for FeB nanoparticle: Molecular dynamics simulation, AIP Advances, 2017, 7(4), 045301.

[78] Tuan Tran Quoc, Dung Nguyen Trong, Molecular dynamics factors affecting

on the structure, phase transition of Al bulk, Physica B: Condensed Matter, 2019, 570, 116–121, 2019.

[79] H. Tsuzuki, P. S. Branicio and J. P. Rino, Structural characterization of deformed crystals by analysis of common atomic neighborhood, Comput. Phys.Commun, 2007, 177, 518–523.

[80] S. Nos´e, A unified formulation of the constant temperature molecular dynamics methods, J. Chem. Phys., 1984, 81, 511–519.

[81] W. G. Hoover, Canonical dynamics: Equilibrium phase-space distributions, Phys. Rev. A, 1985, 31, 1695–1697.

[82] Daniel J. Lacks, First-order amorphous-amorphous transformation in silica, Physical Review Letters, 2000, 84, 4529-4532

[83] G. Guitierrez and B. Johansson, Molecular dynamics study of structural properties of amorphous Al2O3, Physical Review B, 2002, 65, 104202-104210.

[84] Vo Van Hoang and Suhk Kun Oh, Annealing effects on structure in amorphous A12O3 models, Physica B, 2005, 364, 225-232.

[85] Vo Van Hoang, Glass of monatomic Lennard-Jones system at nanoscale, Physica B: Condensed Matter, 2010, 405, 1908-1914.

[86] Vo Van Hoang, T. Odagaki and M. Engel, Cooling rate effects on structure and thermodynamics of amorphous nanoparticles, Applied Surface Science, 2008, 254, 7531-7534.

[87] P. K. Hung, D. K. Belashchenko, V. M. Chieu, N. T. Duong, V. V. Hoang and T. B. Van, Local structure of amorphous canonical systems, Journal of Metastable and Nanocrystalline Material, 1999, 2-6, 393-398.

[88] P. K. Hung, P. N. Nguyen, T. V. Mung, On the estimation of hydrogen diffusion parameters in amorphous and crystalline irons, Journal of Non-Crystalline Solid, 2010, 356, 1262-1266.

[89] J. Li Modell, AtomEye: an efficient atomistic configuration viewer, Simul. Mater. Sci. Eng., 2003, 11, 173.

[90] G. J. Ackland and A. P. Jones, Applications of local crystal structure measures in experiment and simulation, Phys. Rev. B: Condens. Matter Mater. Phys., 2006, 73, 054104.

[91] P. J. Steinhardt, D. R. Nelson and M. Ronchetti , Phys. Rev. B: Condens. Matter Mater. Phys., 1983, 28, 784-805.